

Integration of electrical resistivity imaging (ERI) and ground-penetrating radar (GPR) methods to identify soil profile around Necatibey Subway Station, Ankara, Turkey

Özgür Aktürk · Vedat Doyuran

Received: 31 May 2013 / Accepted: 20 February 2015 / Published online: 1 March 2015
© Springer-Verlag Berlin Heidelberg 2015

Abstract Electrical Resistivity Imaging (ERI) and Ground-Penetrating Radar (GPR) methods were utilized in this study to identify soil profiles around Necatibey Subway Station of Kızılay–Çayyolu metro line, Ankara, Turkey. The Necatibey Metro Station is located within the alluvial deposits of Dikmen stream and the so-called Ankara clay. At the metro station, a number of boreholes were drilled. However, due to the spacing of the boreholes the boundary between alluvium and Ankara clay deposits could not be separated precisely. Thus, in this study, ERI and GPR methods were utilized to distinguish soil types at the study area. GPR measurements were taken from a total of 14 profiles and total length of the profiles was about 320 m. For every ERI measurement section, Schlumberger Dipole–Dipole, Dipole–Dipole, Schlumberger and Wenner arrays were used. Results from the geophysical measurements identified that the fill materials are underlain by the Dikmen stream channel deposits, which consist of silty clay and gravelly sand units. The study also shows that the Dikmen stream channel deposits are underlain by the Ankara clay unit. The meaningful range of resistivity values was between 1 and 15 Ω m, and the GPR signals were strong in sandy units while they attenuated in clayey environments. Based on borehole logs, ERI and GPR data, three-dimensional lithological subsurface model of the survey area was constructed. The resultant three-dimensional diagrams may serve engineers as a practical tool

during different construction stages, groundwater–surface water interactions within short and long term, and probable remedial measures.

Keywords Electrical resistivity imaging · Ground-penetrating radar · Three-dimensional subsurface model · Necatibey subway station · Soil profile

Introduction

It is common for major cities (e.g., the city of Ankara) to be founded on alluvial deposits of clays, silts and sands, usually classified as soft ground. The high cost of urban space in such areas has significantly increased the demand for underground structures. Ground movements induced by excavation of tunnels at urban areas can be transmitted to the ground surface and to predict those movements (deformations), engineers need to identify soil profile precisely first. Identifying critical soil profiles at the working area is the basis of any tunneling project. Although boring logs are very helpful to identify subsurface profile at the working area, the further help of geophysical investigation is always needed to fill the gaps between boreholes arising from the heavily settled areas. Geophysical techniques can be used to identify subsurface geometries due to contrasts in the physical properties. These properties, such as density, magnetic susceptibility, electrical resistivity and conductivity, vary between the media involved, and materials such as limestone, gypsum, siltstone, clay, sand, breccia, air and water all have different geophysical properties (Nouioua et al. 2013). Consequently, geophysical surveys are commonly applied for the detection of different types of subsoil anomalies. Techniques used include seismic reflection and refraction (Cook 1965),

Ö. Aktürk (✉)
Department of Geological Engineering, Akdeniz University,
Dumlupınar Blvd., 07058 Antalya, Turkey
e-mail: akturko@akdeniz.edu.tr

V. Doyuran
Department of Geological Engineering, Middle East Technical
University, Inonu Blvd., 06531 Ankara, Turkey

gravimetry (Colley 1963; Butler 1984; Bishop et al. 1997; Rybakov et al. 2001), ground-penetrating radar (Ballard 1983; Annan et al. 1991) and resistivity tomography (Zhou et al. 2002).

Electrical Resistivity Imaging (ERI) and Ground-Penetrating Radar (GPR) are among the most popular near-surface geophysical methods, especially with the advancement in equipment and computing technology. Generally, they are time- and cost-effective and relatively easy to execute. Both methods are affected by the ground conductivity. This physical parameter provides the means with which the methods can be integrated as the main parameter governing the application principles of ERT techniques and highly affects the propagation of the GPR signals.

Electrical resistivity, also called DC resistivity prospecting, is one of the oldest and most popular geophysical techniques in the field of near-surface geophysics. During the last two decades, the technique has been improved in terms of data acquisition systems, i.e., the development of multi-electrode and capacitive-coupled resistivity systems and processing software. After these developments, the method has been more frequently referred to as ERI. ERI has been widely applied in environmental and engineering geophysics to obtain 2D and 3D high-resolution images of the resistivity subsurface patterns (Suzuki et al. 2000; Caputo et al. 2003; Martínez et al. 2009, 2012; Rey et al. 2013). Although ERI is a useful tool in mineral exploration (Sasaki and Matsuo 1993; Van Schoor and Duvenhage 2000), the technique is well suited to applications in the fields of hydrogeology, environmental science and engineering (Spies and Ellis 1995; Barker and Moore 1998). The ERI technique provides a direct and exact determination of the depth attained in the survey. This is due to the fact that the depth of investigation is mainly controlled by the theoretical relationships between electrode spacing and geometry for a homogeneous earth medium. Assuming that the procedure does not depend on external factors such as water content or lithology the depth to the anomalies can be directly estimated (Griffiths and Barker 1993; Reynolds 1997; Gómez-Ortiz et al. 2007).

Ground-penetrating radar (GPR) has proven to be a useful geophysical tool in the characterization of physical properties, thickness, spatial distribution, internal structures and discontinuities of subsurface materials (Russell and Stasiuk 1997; Rust and Russell 2000; Cagnoli and Russell 2000; Cagnoli and Ulrych 2001a, b; Miyamoto et al. 2003; Gómez-Ortiz et al. 2006, 2007; Jol 2009; Kadioglu et al. 2013). GPR detects electromagnetic discontinuities in the shallow subsurface (generally less than 20 m depth) by the generation, propagation, reflection and reception of high-frequency electromagnetic pulses. GPR is used in geological investigations to define lithological

contacts (e.g., Jol and Smith 1991; Pratt and Miall 1993), locate faults (e.g., Rashed et al. 2003; Slater and Niemi 2003; Gross et al. 2004; Yalçınır et al. 2013), interpret soil profiles (e.g., Doolittle and Collins 1995), to study sub-glacial topography (e.g., Overgaard and Jakobsen 2001) and to estimate the depth to groundwater (e.g., Beres and Haeni 1991; Menezes Travassos and Luiz Menezes 2004). This technique has been also applied to the study of volcanic deposits and related volcanic hazards (Russell and Stasiuk 1997; Rust and Russell 2000; Cagnoli and Russell 2000; Cagnoli and Ulrych 2001a, b; Miyamoto et al. 2003; Gómez-Ortiz et al. 2006).

The focus of this study is to construct the subsurface soil profiles around Ankara Subway System Necatibey Station and its close vicinity. This study mainly aims at applying ERI and GPR techniques to fill the gaps between boreholes at the area of interest. As a result of correlations among boring logs, ERI and GPR results, three-dimensional lithological subsurface model of the survey area was constructed. The resultant three-dimensional diagrams may serve engineers as a practical tool during different construction stages, groundwater–surface water interactions within short and long term, and preventive measures.

Materials and methods

Study area and geological settings

The study area is the Ankara Subway System Kızılay-Çayyolu Line Necatibey Station (Ankara, Turkey) located among the buildings of Turkish General Staff, Turkish Air Force and General Directorate of Highways (Fig. 1).

Necatibey Station is about 140 m long. It has two horseshoe-shape main tunnels each 9 meters high and 11 meters wide. There are also four connecting tunnels between them. Above the tunnel floor, the construction of a pedestrian floor and a shopping center is expected. Three escalators are also planned for the pedestrians.

Since the tunneling project is located among residential, governmental and military buildings, the project works had to be performed under extreme care not to damage any of the surrounding structures above the ground or service infrastructure found below the ground as well as not to interfere with the daily lives of the populace within the vicinity of the neighborhood. Passing by many important residential and governmental areas the project would have a major effect on the city of Ankara. Although the project is designed to make this a positive one, a minor mistake in the engineering applications can cause a major damage in the critical area.

To reveal the geology along the Necatibey Station a number of boreholes were planned. A total of 11 boreholes

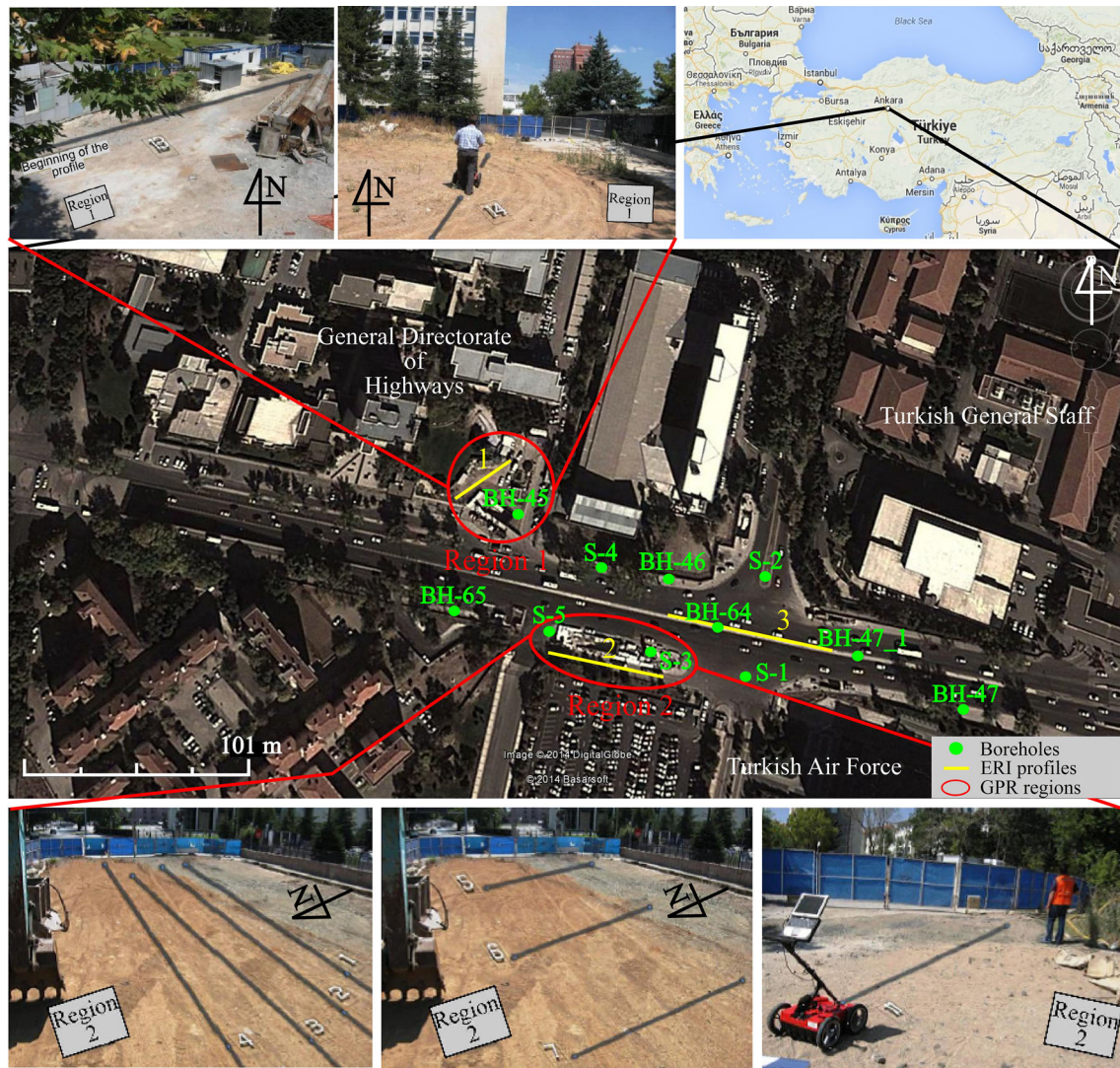


Fig. 1 Study area showing ERI profiles (solid yellow lines) and GPR locations (red circles) and borehole locations (green dots)

were drilled (TOKER Drilling and Construction Co. 2003) to assess and evaluate the soil type, thickness, contact relationships, geological and geotechnical properties of lithological units present along the Necatibey Station. Details regarding these boreholes are given in the dissertation by Aktürk (2010). By considering soil groups (according to Unified Soil Classification System), color index and SPT values, the units belonging to alluvium and Ankara clay (Gölbaşı formation) were separated. The alluvium of the Dikmen Valley cuts Necatibey Station almost perpendicularly and is composed of clay, silty clay and gravelly sand units. The Ankara clay is dominantly composed of silty and/or sandy clays with occasional sand and gravel lenses. Even though fine-grained deposits are dominant, the sand and gravel lenses are also encountered. The Ankara clay is of Pliocene age (TOKER Drilling and Construction Co., 2003). It is basically silty clay and

gravelly, sandy clay that is red, brown and beige, fissured, contains carbonate concretions, and partly has layers of sand and gravel, both low and high in plasticity, very stiff and over-consolidated.

Electrical resistivity imaging

ERI is based on injecting electrical current into the subsurface using a pair of electrodes (current electrodes) and measuring the potential between another pair of electrodes (potential electrodes). The measured potential allows for the determination of values of resistance, which are then converted into apparent resistivity by multiplying the resistance by an appropriate geometric factor. The geometric factor depends on the type of acquisition array being used (Sheriff 1999). The apparent resistivity is then inverted to obtain the true subsurface resistivity and to reveal the

thickness and depth of individual resistivity layers within the subsurface. Inversion is a fundamental step in all modern resistivity imaging surveys. It is, basically, a mathematical procedure by which the subsurface physical parameter distribution is estimated based on a set of field measurements (Telford et al. 1990; Reynolds 2000; Loke and Barker 1995).

The method consists of placing electrodes along profiles using a specific spacing that depends on the required resolution, depth and the purposes of the study. A higher resolution is obtained if the electrodes are placed closer, while for widely spaced electrodes, a greater depth can be imaged or investigated (Sasaki 1992). Technically, an electrical resistivity imaging survey can be carried out using different electrode arrays (e.g., dipole–dipole, Wenner, Schlumberger, Wenner–Schlumberger) that are spread across the surface. The characteristics and specifications of each array and also suggestions about choosing the most effective array can be found in Zhou and Dahlin (2003), Dahlin and Zhou (2004), and Drahor (2006).

The electrodes were connected to a measuring device and its specific control system was used to select the group of electrodes that should function simultaneously in a particular electronic arrangement. For each arrangement, the resistivity was measured and attributed to a specific geometric point in the subsurface. ERI equipment used in this research was the ARES Automatic Resistivity System manufactured by GF Instruments, S.R.O. This multi-electrode equipment consists of an integrated computer capable of managing up to 200 electrodes and a transmitter possessing power up to 850 W, current up to 5 A, voltage 2000 V_{p-p} (actually applied voltage automatically level of measured potential).

The exact locations of resistivity profiles were superimposed using solid yellow lines as illustrated in Fig. 1. Lack of space for the extension of multi-electrode cables is attributed to the densely populated residential area. The profile lengths were 30 m with 2 m electrode spacing for profile 1; 52.5 m with 3.5 m electrode spacing for profile 2 and 75 m with 5 m electrode spacing for profile 3.

For every profile, four different electrode arrays whose advantages and disadvantages will be further expatiated upon were utilized. These were namely (a) Schlumberger N6 Dipole Dipole N4, (b) Dipole Dipole N6 S1, (c) Schlumberger N6, and (d) Wenner Alpha. The letters N, S and Alpha are geometric factors related with different electrode configurations indicating the ratio of distance between current and potential electrodes to the dipole length. The measured resistivity data were then need to be inverted to get true resistivity values of the subsurface. To invert measured resistivity values RES2DINV (2004) inversion software was used. This program uses the conditioned least squares smoothing method modified with the quasi-Newton

optimization technique. The inversion procedure creates an underground model using rectangular prisms and determines the values of resistivity for each of these prisms, minimizing the difference between observed and calculated apparent resistivity values (Loke and Barker 1996; Loke and Dahlin 2002).

Ground-penetrating radar

In GPR, a transmitting antenna radiates an electromagnetic pulse into the ground that is transmitted, reflected, and diffracted by features corresponding to changes in the electrical properties of the earth. The waves that are reflected and diffracted back toward the earth's surface may be detected by a receiving antenna, amplified, digitized, displayed, and stored for further analysis. The time it takes for the wave to return can be measured and converted into distances between the targets and the antennas (Daniels et al. 1988; Davis and Annan 1989). By analyzing some of characteristic properties of the returned pulse, small details (e.g., dimensions) and significant information (e.g., depth) about the target and ultimately the subsurface can be obtained (Daniels et al. 1988; Davis and Annan 1989).

GPR signals are electromagnetic waves, which are electronic excitation of a dipole and propagate, at high frequency, typically between 10 and 1000 MHz, as a periodic disturbance. Electromagnetic waves have both electric and magnetic components, which are perpendicular to each other. Since subsurface geological materials have different electrical and magnetic properties it is possible to exploit GPR to map the variations in some of these properties, and therefore characterize the subsurface geology. The penetration depth and the resolution depend on the electromagnetic properties of the geological materials through which the electromagnetic waves propagate and on the type of antenna that is used. Therefore, subsurface wave propagation decreases as the conductivity of the terrain or the frequency of the emitted signal increases. For a single profile, a higher carrier frequency of the antennas results not only in a higher resolution but also in a decreased penetration depth, and vice versa if the frequency decreases (Davis and Annan 1989).

A Cobra Locator GPR system produced by Radarteam Sweden AB was used to conduct or execute this study. The system consists of three main units: a control unit, to collect and process data, a monitor for storage and visualization at high speed, and the antenna. The control unit has a 10.8 V battery, Ethernet communication with the monitor, two auxiliary ports for connecting external devices. The Cobra Locator has dual shielded antennas with integrated 2-channel GPR system. Peak frequency is 250 MHz and the operating bandwidth is between 100 and 900 MHz.

Primary field assessments led to the choice of 64- and 128-ns temporal sampling intervals. Data were gathered using GAS data capture software. GPR surveys were planned at almost the same locations (Fig. 1; region 1 and 2) as the electrical resistivity survey, to make good correlation of data. Study locations were denoted as regions 1 and 2 and data gathered in different directions within every region. While planning profile directions it was attentive to take measurements from parallel and perpendicular profiles to construct three-dimensional images of soil at the study area. Figure 1 shows survey profile numbers at regions 1 and 2. As seen from the Fig. 1, GPR measurements were taken from a total of 14 profiles and total length of the profiles was about 320 m. During GPR measurements on aforementioned profiles at different regions, some data gathering specifications were as follows: time window: 64 and 128 ns; data gain: 5 dB (start), 15 dB (end); bandpass filter with cutoff frequencies of 130 and 700 MHz; trace frequency: 25 trace/sec.; offset: 18 ns; data output: 16 bit. To process raw data, GPRSoft (2008) data processing software was utilized. More about the processing of the GPR data can be found in Daniels et al. (1988), Young et al. (1995), Conyers and Goodman (1997), Annan (1999, 2002, 2003), Jol and Kaminsky (2000), Reynolds (2000) and Alshuhail (2006).

Experimental results

Electrical resistivity imaging

The model of the soil was obtained by an inversion process based on an iterative method that attempts to minimize the difference between the measured pseudo-section and a pseudo-section recalculated from a model of electrical resistivity theory. In general, the more reliable model is located just after the iteration where the root mean-squared ‘RMS’ error does not change significantly (<0.5 % improvement), which usually happens between four and six iterations (Nouioua et al. 2013).

After the inversion process, resultant 2D resistivity images as illustrated from Figs. 2, 3, and 4 were interpreted. Results from the 2D resistivity images were compared with the boring log data to depict how well the ERI correlates the borehole information. As mentioned before, four different array configurations were used for every profile and the letters a, b, c and d indicate these different electrode configurations for the same profile.

The length of profile 1 was 30 m with 2 m electrode spacing as illustrated in Fig. 2. Since penetration depth is directly proportional to profile length and electrode spacing, the penetration depth for profile 1 was limited and was about 5 m. First 1–1.5 m was interpreted as “fill” due to

the resistivity values between 9 and 15 Ω m. After 1.5 m depth, “clayey soil” took place up to deepest point of the Section (5 m) with 2–3 Ω m resistivity values. The closest boring log to the profile 1 is BH 45 and the lithology constructed by interpreting profile 1 resistivity values is reasonably in agreement with the BH 45 log for the uppermost 5 m.

Figure 3 illustrates 2D resistivity image for profile 2. As seen, profile length was 52.5 m and reachable depth was about 9 m. First 3–4 m depth was occupied by “fill material” with 5–13 Ω m resistivity values. This part (3–4 m) was underlain by “wet clayey soil” with low resistivity values (less than 5 Ω m). The closest borehole logs (S3 and S5) are in a good agreement with interpretation of profile 2 resistivity values.

2D resistivity image for profile 3 is illustrated in Fig. 4. The length and depth of the profile are 75 and 12.5 m, respectively. It was thought that first 7–8 m occupied by “fill material” and after that depth “silty clayey alluvium” took place. The abrupt increase in resistivity values at 4–5 m depth may indicate a concrete structure. BH 64 is the closest borehole to the profile and its log is compatible with the resistivity interpretations.

At this point, it should be kept in mind that all interpretations mentioned above are site specific. For example, resistivity values between 5 and 15 Ω m were attributed to “fill material” since ongoing excavation works at the site gave observation opportunity very well. Similarly, simultaneous dewatering works supplied clues about original and lowered water head. That is why resistivity values less than 5 Ω m were evaluated as wet clayey soil at profile 2. Also contribution of boring logs cannot be ignored especially for the interpretation of profile 3.

As shown in Figs. 2, 3 and 4, the shape of the contours in the pseudo-section produced by the different arrays over the same structure can be very different. The choice of the “best” array for a field survey depends on the type of structure to be mapped, the sensitivity of the resistivity meter and the background noise level. Among the characteristics of an array that should be considered are (1) the depth of investigation, (2) the sensitivity of the array to vertical and horizontal changes in the subsurface resistivity, (3) the horizontal data coverage and (4) the signal strength. The Wenner array is an attractive choice for a survey carried out in a noisy area (due to its high signal strength) and also if good vertical resolution is required. The dipole–dipole array might be a more suitable choice if good horizontal resolution and data coverage are important (assuming the resistivity meter is sufficiently sensitive and there is good ground contact). The Wenner–Schlumberger array (with overlapping data levels) is a reasonable all-round alternative if both good and vertical resolutions are needed, particularly if good signal strength is also required.

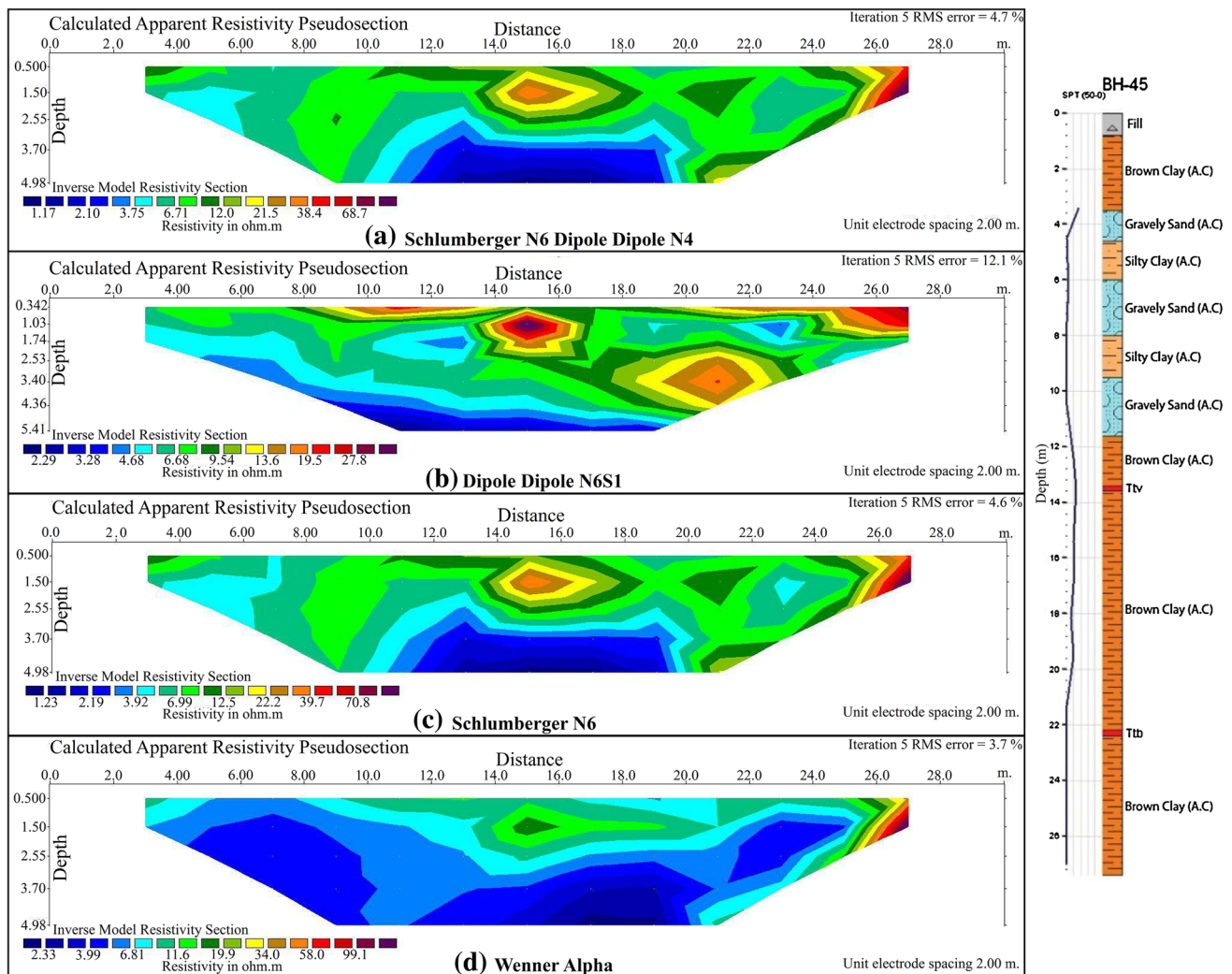


Fig. 2 Interpretation of **a** Schlumberger N6 Dipole Dipole N4, **b** Dipole Dipole N6S1, **c** Schlumberger N6, **d** Wenner Alpha electrode configurations for profile 1 and BH 45 boring log

If a system with a limited number of electrodes is used, the pole–dipole array with measurements in both the forward and reverse directions might be a viable choice. For surveys with small electrode spacing and require a good horizontal coverage, the pole–pole array might be a suitable choice.

Ground-penetrating radar

GPR results are very site specific because of the limited depth of penetration of radar in conductive environments, such as in clay and freshwater bearing sediments as it was in the study area. The amplitude of EM fields decreases exponentially with depth. In most materials, energy is lost due to scattering from material variability. The signal propagates well in sand and gravel while conductive soils such as clay, or fill saturated with conductive groundwater

cause GPR signal attenuation and loss of penetration depth, i.e., limited detection of deeper objects (Reynolds 2000; Annan 2003; Olhoeft et al. 1994).

In a general sense, at two regions identified in the study area, clayey and alluvium units were observed after 1–1.5 m depth. These units can be seen especially at Region 2, profiles 11, 12 (Figs. 5, 6). Other bands (above dashed lines in Figs. 5, 6) observed in the radagrams can be interpreted as sandy units since GPR signals continue their travel ideally within sandy environment while they attenuate within alluvium, clayey and wet strata.

A three-dimensional view of subsurface profile at Region 2 was constructed by carefully combining parallel or orthogonal 2D profiles and considering their positions and scale in the GPRSoft (2008) software environment rather than acquiring a true 3D dataset and the resultant image is illustrated in Fig. 7. As implemented by McMechan et al.

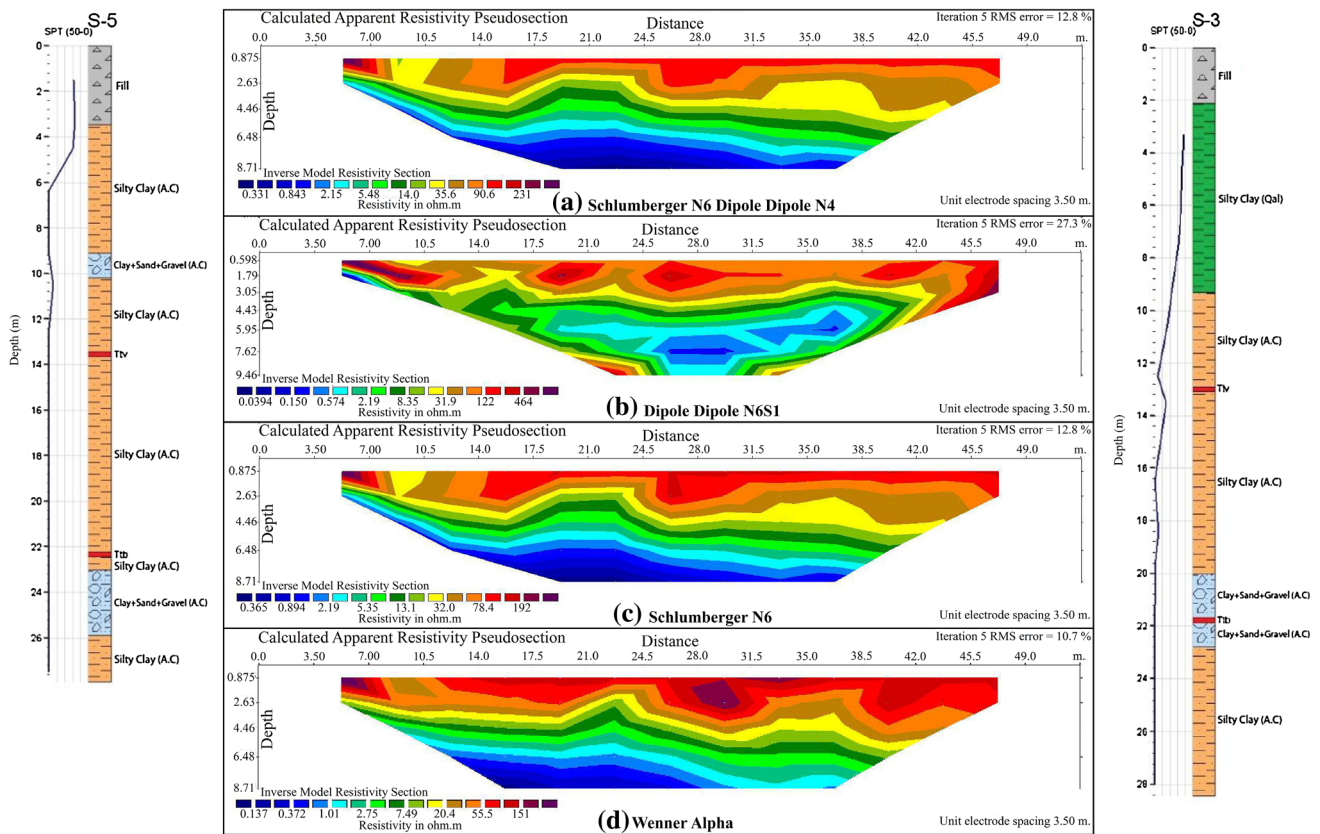


Fig. 3 Interpretation of **a** Schlumberger N6 Dipole Dipole N4, **b** Dipole Dipole N6S1, **c** Schlumberger N6, **d** Wenner Alpha electrode configurations for profile 2 and S3, S5 boring logs

(1997), Jol and Kaminsky (2000) and Cristallini and Al-mendinger (2001), the interpretable pseudo-3D volume can be constructed by combining the individually processed 2D profiles. It should be also stated that no interpolation method was applied since there were little differences in distance between adjacent profiles.

Figure 7 shows that there exists compressed sandy fill (showing strong reflections) up to 1 m in all profiles. Although it is not possible to determine that the anomaly is “compressed sandy fill” only by means of GPR data, site observations and ERI result contributions were also evaluated. After 1 m, almost all profiles consist of clayey and alluvium (showing weak reflections) units and sandy (showing strong reflections) units. Additionally, profiles 5, 6, 7, 8, 9, 10 show scattered signals in their FFT (Fast Fourier Transform) algorithms and chosen window FFT algorithms (linear and logarithmic), especially close to the surface. That proves alluvium accumulation at the site occurred in the same direction with profiles 5, 6, 7, 8, 9 and 10. Furthermore, from profile 1 to profile 4 at Region 2, the thickness of the clayey and alluvium units tends to increase. In the same direction, at Region 1, clayey and alluvium units can be seen densely especially after 1–1.5 m depth. By considering the depth and

thickness of the units it can be concluded that the clayey and alluvium units are getting thicker from South to North at the study area. The interpretations about alluvium accumulation direction are compatible with the average slope of the Dikmen Valley and the flat lying topography at the site.

For data processing, all data were subjected to background removals and during this process, the first 50–60 cm part of scanning surface was considered as compressed unit. For better understanding of the effect of this part on results, efficiency indexes were chosen as follows: (1) wide for 0–10 ns, (2) mean for 10–20 ns and (3) 25 % higher than mean value for 20 ns and below. Identified efficiency indexes were 50 units for 0–10 ns, 100 units for 10–20 ns and 125 units for 20 ns and below. Also, since the GPR device used in this study has wheel triggering mechanism, all data were gathered using distance mode and therefore distance/velocity analysis was not applied while data processing.

Integration of ERI, GPR and borehole logs

With the interpretation of ERI, GPR and boring logs data together, the regional 3D subsurface panel diagrams were

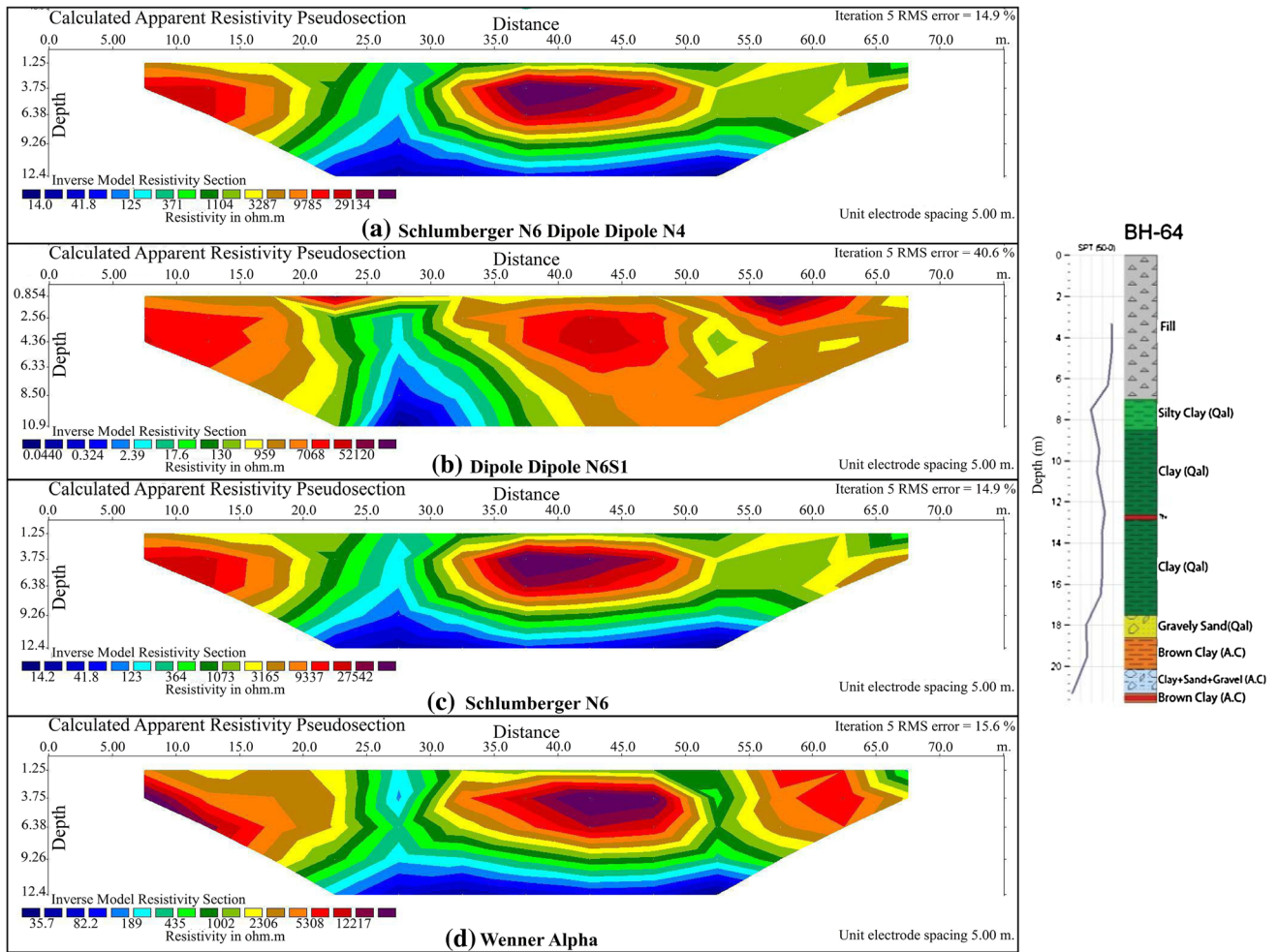


Fig. 4 Interpretation of **a** Schlumberger N6 Dipole Dipole N4, **b** Dipole Dipole N6S1, **c** Schlumberger N6, **d** Wenner Alpha electrode configurations for profile 3 and BH 64 boring log

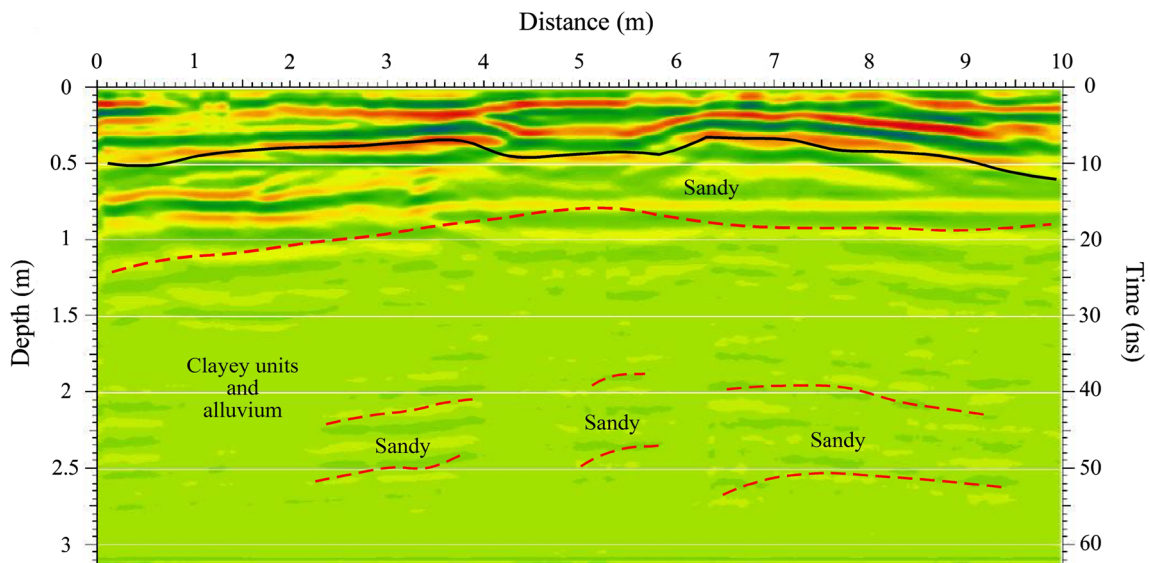


Fig. 5 Radagram from Region 2, profile 11

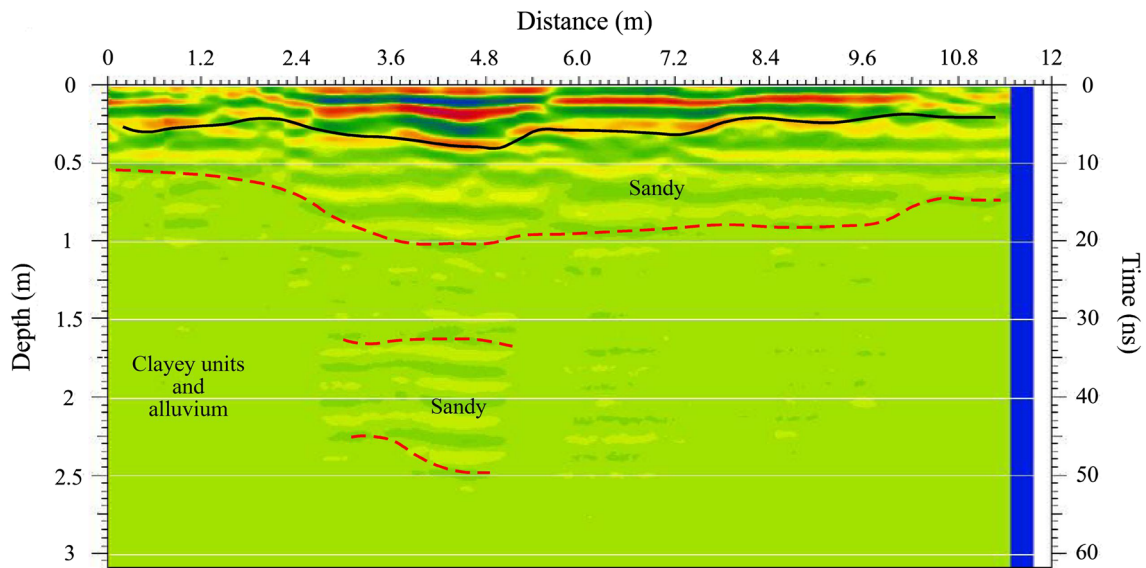


Fig. 6 Radagram from Region 2, profile 12

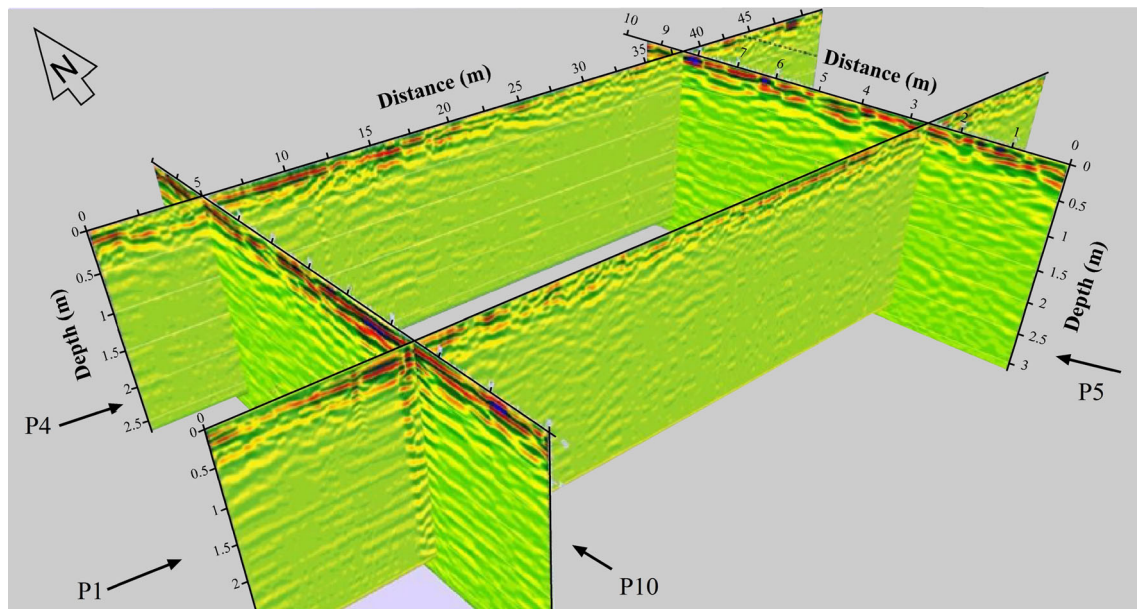


Fig. 7 Three-dimensional view of GPR results at Region 2

constructed using RockWorks software (RockWorks 2009) and presented in Fig. 8. For creating 3D subsurface panel (fence) diagrams, first of all, soil models deduced from geophysical (ERI and GPR) and boring logs data were introduced to the borehole manager tool of the software to interpolate a solid model of the lithology data and to create a 3D fence diagram that illustrates the lithology model. The different lithologies are color-coded based on their background color in the Lithology Type Table of the software. During the process of building the fence panels, the software creates a solid model by itself for the lithology of the

entire project and then displays the lithologies present on the selected fence panel. Solid modeling is a built-in and a true 3D gridding process in which a solid modeling algorithm (e.g., closest point, distance to point or inverse-distance weighting, etc.) is used to extrapolate G values (e.g., geophysical measurements, geochemical concentration, or any other downhole or subsurface quantitative value) for a fixed X (Easting), Y (Northing) and Z (elevation) coordinates. In this study, G values were soil models interpreted from ERI and GPR. Once it knows the dimension of the study area, the software divides it into 3D cells

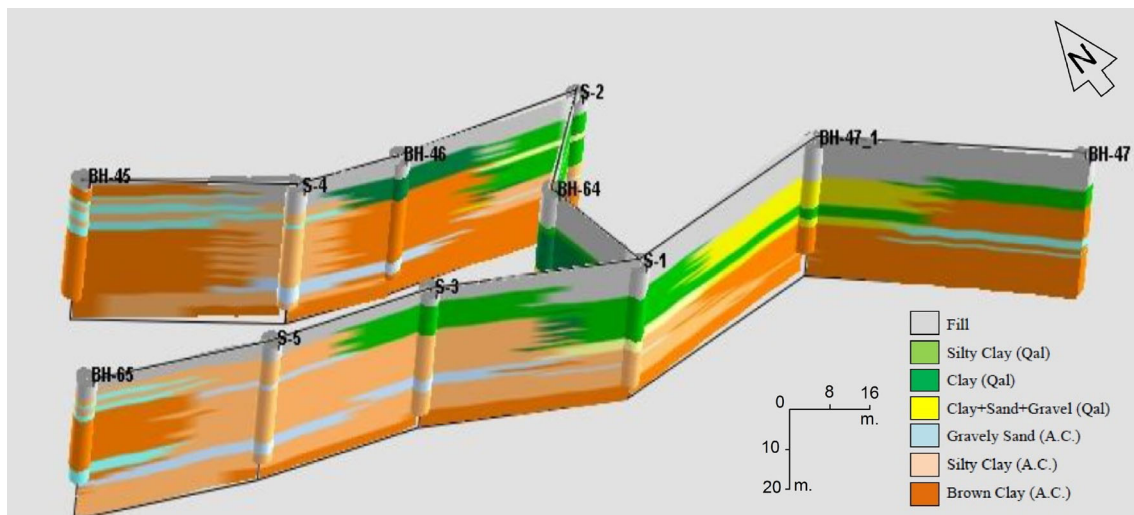


Fig. 8 Regional 3D subsurface panel diagram created by interpreting ERI, GPR and borehole logs together

automatically or user defined. Each cell is defined by its corner point or node. Each node is assigned the appropriate X , Y and Z location coordinates according to its relative placement within the area of interest. The fourth variable G is estimated based on the G value of the given data points between boreholes to construct panels.

Conclusions and problem discussion

The Necatibey Station of the Ankara Subway System is located within the alluvial deposits of Dikmen Creek and the so-called Ankara clay. At the subway station a number of boreholes were drilled. However, due to the spacing of the boreholes the boundary between alluvium and Ankara clay deposits could not be separated precisely. Thus, in this study, ERI and GPR studies have been conducted for the delineation of the boundaries of the two deposits.

One of the effective difficulties associated with ERI was finding sufficient space for the layout of the cables. The study area is located among the buildings of Turkish General Staff, Turkish Air Force and General Directorate of Highways. Due to dense settlement and restrictions imposed by the military buildings available space was highly limited for the layout of the multi-electrode cables. This was the main reason for limited depth of penetration. Reachable penetration depth was 5 m for the 30-m-long profile 1, 9 m for the 52.5-m-long profile 2 and 12.5 m for the 75-m-long profile 3. A conductive layer should conduct more current flow (hence deeper penetration depth) while a resistive layer should resist current flow (hence shallower penetration depth). The resistivity contrast between Ankara clay and the Dikmen Valley alluvium was not significantly high because of high clayey content of the alluvium as well. Wet clayey soils were identified with its 2–3 Ωm

resistivity values. The sandy and gravelly lenses within the Ankara clay would also respond similarly to those of alluvium. From the resistivity profiles, it is confirmed that the foundation soil of the metro station is highly heterogeneous. In the model, this heterogeneity is smoothed out by defining a transition zone between the Ankara clay and the alluvial deposits.

GPR results are very site specific because of the limited depth of penetration in conductive environments, such as in clay- and water-bearing sediments as it is in the study area. The amplitude of EM fields decreases exponentially with depth. In most materials, energy is lost to scattering from material variability. The signal propagates well in sand and gravel while conductive soils such as clay or fill saturated with conductive groundwater cause GPR signal attenuation and loss of target resolution. Because of high clay content of the foundation soils, penetration depth of GPR was rather limited. By considering the depth and thickness of the clayey and alluvium units at the area of interest, it can be concluded that the clayey and alluvium units are getting thicker from South to North at the study area.

With the interpretation of geophysical tests (ERI and GPR) and borehole logs together, the regional 3D subsurface panel diagrams were constructed. Such panel diagrams were produced using borehole logs for engineering projects. The contributions of ERI and GPR data in this study improve the confidence level of the panel diagrams without doubt. The resultant 3D diagrams are expected to serve engineers as a practical tool during different construction stages, groundwater–surface water interactions within short and long term, and probable remedial measures.

Acknowledgments This paper is dedicated to the great memory of the second author Prof. Dr. Vedat Doyuran who passed away unexpectedly just after the original manuscript was sent for review. Authors are grateful to Dr. A. Arda Özacar and Mr. Ertuğ Çelik for

their contributions during fieldworks. Thanks are also due to Dr. Çağıl Kolat for her help to reinterpret boring logs. Authors are also indebted to the anonymous reviewers for their constructive comments. Funding for this project was provided by Scientific Research Development Program at Middle East Technical University and Akdeniz University, and these supports are gratefully acknowledged.

References

- Aktürk Ö (2010) Assessment of Tunnel Induced Deformation Field Through 3-Dimensional Numerical Models (Necatibey Subway Station, Ankara, Turkey). Ph.D. Dissertation, the Graduate School of Natural and Applied Sciences of Middle East Technical University
- Alshuhail AA (2006) Integration of 3D Resistivity Imaging and Ground Penetrating Radar Surveys in Characterizing Near-Surface Fluvial Environment. Master Thesis, University of Calgary, Department of Geology and Geophysics, Alberta
- Annan AP (1999) Practical Processing of GPR Data. Proceeding of the Second Government Workshop on Ground Penetrating Radar, Mississauga 16 pp
- Annan AP (2002) The History of Ground Penetrating Radar. *Subsurf Sens Technol Appl* 3(4):303–320
- Annan AP (2003) Ground penetrating radar: principles, procedures and applications. Sensor and Software Inc, Mississauga, p 271
- Annan AP, Cosway SW, Redman JD (1991) Water table detection with ground-penetrating radar. In: *Soc Explor Geophys. Annual International Meeting Program with Abstracts*, pp 494–497
- Ballard RF (1983) Cavity detection and delineation research. Report 5, Electromagnetic (radar) techniques applied to cavity detection. Technical Report GL, 83–1, p 90
- Barker R, Moore J (1998) The application of time-lapse electrical tomography in groundwater studies. *Lead Edge* 17(10):1454–1458
- Beres M, Haeni FP (1991) Application of ground-penetrating-radar methods in hydrogeologic studies. *Ground Water* 29:375–386
- Bishop I, Styles P, Emsley SJ, Ferguson NS (1997) The detection of cavities using the microgravity technique: case histories from mining and karstic environments. *Geol Soc Eng Geol Spec Publ* 12:153–166
- Butler DK (1984) Microgravimetric and gravity gradient techniques for detection of subsurface cavities. *Geophysics* 49(7):1084–1096
- Cagnoli B, Russell JK (2000) Imaging the subsurface stratigraphy in the Ubehe hydrovolcanic field (Death Valley, California) using ground penetrating radar. *J Volcanol Geotherm Res* 96:45–56
- Cagnoli B, Ulrych TJ (2001a) Ground penetrating radar images of unexposed climbing dune-forms in the Ubehebe hydrovolcanic field (Death Valley, California). *J Volcanol Geotherm Res* 109:279–298
- Cagnoli B, Ulrych TJ (2001b) Singular value decomposition and wavy reflections in ground penetrating radar images of base surge deposits. *J Appl Geophys* 48:175–182
- Caputo R, Piscitelli S, Oliveto A, Rizzo E, Lapenna V (2003) High-resolution resistivity tomographies in active tectonic studies. Examples from the Tyrnavos Basin, Greece. *J Geodyn* 36:19–35
- Colley GC (1963) The detection of caves by gravity measurements. *Geophys Prospect* XI: 1–9
- Conyers LB, Goodman D (1997) *Ground Penetrating Radar*. Altamira Press, An Introduction for Archaeologist
- Cook JC (1965) Seismic mapping of underground cavities using reflection amplitudes. *Geophysics* 30(4):527–538
- Cristallini E, Almendinger R (2001) Pseudo 3D Modeling of Trishear Fault-Propagation Folding. *J Structural Geology* 23:1883–1899
- Dahlin T, Zhou B (2004) A numerical comparison of 2D resistivity imaging with 10 electrode arrays. *Geophys Prospect* 52:379–398
- Daniels DJ, Gunton DJ, Scott HF (1988) Introduction to Subsurface Radar. *IEEE Proc F* 135:278–320
- Davis JL, Annan AP (1989) Ground Penetrating Radar for High Resolution Mapping of Soil and Rock Stratigraphy. *Geophys Prospect* 37:531–551
- Doolittle JA, Collins ME (1995) Use of soil information to determine application of ground penetrating radar. *J Appl Geophys* 33:101–108
- Drahor MG (2006) Integrated geophysical studies in the upper part of Sardis archaeological site, Turkey. *J Appl Geophys* 59:205–223
- Gómez-Ortiz D, Martín-Velázquez S, Martín-Crespo T, Márquez A, Lillo J, López I, Carreño F (2006) Characterization of volcanic materials using ground penetrating radar: a case study at Teide volcano (Canary Islands, Spain). *J Appl Geophys* 59(1):63–78
- Gómez-Ortiz D, Martín-Velázquez S, Martín-Crespo T, Márquez A, Lillo J, López I, Carreño F, Martín-González F, Herrera R, De Pablo MA (2007) Joint application of ground penetrating radar and electrical resistivity imaging to investigate volcanic materials and structures in Tenerife (Canary Islands, Spain). *J Appl Geophys* 62:287–300
- GPRSoft (2008) Version 1.3.7. Geoscanners AB. www.geoscanners.com
- Griffiths DH, Barker RD (1993) Two-dimensional Resistivity Imaging and Modeling in Areas of Complex Geology. *J Appl Geophys* 29:211–226
- Gross R, Green AG, Horstmeyer H, Begg JH (2004) Location and geometry of the Wellington Fault (New Zealand) defined by detailed three-dimensional georadar data. *J Geophys Res* 109:B05401. doi:10.1029/2003JB002615
- Jol HM (2009) *Ground Penetrating Radar: Theory and Applications*. Elsevier B.V, Amsterdam
- Jol HM, Kaminsky G (2000) High Resolution 2D and 3D Ground Penetrating Radar Datasets. US Geological Survey, Open-File Report: 99–104
- Jol HM, Smith DG (1991) Ground penetrating radar of northern lacustrine deltas. *Can J Earth Sci* 28:1939–1947
- Kadioglu S, Kadioglu M, Kadioglu YK (2013) Identifying of buried archeological remains with ground penetrating radar, polarized microscope and confocal Raman spectroscopy methods in ancient city of Nysa, Aydin-Turkey. *J Archeol Sci* 40(10):3569–3583
- Loke MH, Barker RD (1995) Least-squares deconvolution of apparent resistivity pseudosections. *Geophysics* 60:1682–1690
- Loke MH, Barker RD (1996) Rapid least-squares inversion of apparent resistivity pseudosections by a quasi-Newton method. *Geophys Prospect* 44:131–152
- Loke MH, Dahlin T (2002) A comparison of the Gauss–Newton and quasi-Newton methods in resistivity imaging inversion. *J Appl Geophys* 49:149–162
- Martínez J, Benavente J, García-Aróstegui JL, Hidalgo MC, Rey J (2009) Contribution of electrical resistivity tomography to the study of detrital aquifers affected by seawater intrusion–extrusion effects: the river Vélez delta (Vélez-Málaga, southern Spain). *Eng Geol* 108:161–168
- Martínez J, Rey J, Hidalgo C, Benavente J (2012) Characterizing abandoned mining dams by geophysical (ERI) and geochemical methods: the Linares–La Carolina District (southern Spain). *Water Air Soil Pollut* 223:2955–2968
- McMechan G, Gaynor G, Szerbiak R (1997) Use of ground penetrating radar for 3D sedimentological characterization of clastic reservoir analogs. *Geophysics* 62:786–796
- Menezes Travassos J, Luiz Menezes P (2004) GPR exploration for groundwater in a crystalline rock terrain. *J Appl Geophys* 55:239–248

- Miyamoto H, Haruyama J, Rokugawa S, Onishi K, Toshioka T, Koshinuma J (2003) Acquisition of ground penetrating radar data to detect lava tubes: preliminary results on the Komoriana cave at Ruji volcano in Japan. *Bull Eng Geol Environ* 62:281–288
- Nouioua I, Rouabhia A, Fehdi C, Boukelloul ML, Gadri L, Chabou D, Mouici R (2013) The application of GPR and electrical resistivity tomography as useful tools in detection of sinkholes in the Cheria Basin (northeast of Algeria). *Environ Earth Sci* 68:1661–1672
- Olhoeft GR, Powers MH and Capron DE (1994) Buried object detection with ground penetrating radar. In: *Proceeding of Unexploded Ordnance Detection and Range Remediation Conference*, 207–233
- Overgaard T, Jakobsen PR (2001) Mapping of glaciectonic deformation in an ice marginal environment with ground penetrating radar. *J Appl Geophys* 47:191–197
- Pratt BR, Miall AD (1993) Anatomy of a bioclastic grainstone megashoal (Middle Silurian, southern Ontario) revealed by ground-penetrating radar. *Geology* 21:223–226
- Rashed M, Kawamura D, Nemoto H, Miyata T, Nakagawa K (2003) Ground penetrating radar investigations across the Uemachi fault, Osaka, Japan. *J Appl Geophys* 53:63–75
- RES2DINV (2004) Version 3.54. Rapid 2D Resistivity and IP inversion using the Least Square Method. Geotomo Software, www.geoelectrical.com
- Rey J, Martínez J, Hidalgo MC (2013) Investigating fluvial features with electrical resistivity imaging and ground-penetrating radar: the Guadalquivir River terrace (Jaen, Southern Spain). *Sediment Geol* 295:27–37
- Reynolds JM (1997) *An introduction to applied and environmental geophysics*. Wiley, Chichester
- Reynolds JM (2000) *An Introduction to Applied and Environmental Geophysics*. Wiley, New York
- RockWorks (2009) Version 2009.2.5. RockWare Incorporated. www.rockware.com
- Russell JK, Stasiuk MV (1997) Characterization of volcanic deposits with ground-penetrating radar. *Bull Volcanol* 58:515–527
- Rust AC, Russell JK (2000) Detection of welding in pyroclastic flows with ground penetrating radar: insights from field and forward modelling data. *J Volcanol Geotherm Res* 95:23–34
- Rybakov M, Goldshmidt V, Fleischer L, Rotstein Y (2001) Cave detection and 4-D monitoring: a microgravity case history near the Dead Sea. *Lead Edge (Soc Explor Geophys)* 20(8):896–900
- Sasaki Y (1992) Resolution of resistivity tomography inferred from numerical simulation. *Geophys Prospect* 40:453–464
- Sasaki Y, Matsuo K (1993) Surface-to-tunnel resistivity tomography at the Kamaishi Mine. *Butsuri-Tansa* 46:128–133
- Sheriff RE (1999) *Encyclopedic Dictionary of Exploration Geophysics*, Society of Exploration Geophysics, 3rd edn
- Slater L, Niemi TM (2003) Ground-penetrating radar investigation of active faults along the Dead Sea Transform and implications for seismic hazards within the city of Aqaba, Jordan. *Tectonophysics* 368:33–50
- Spies B, Ellis R (1995) Cross-borehole resistivity tomography of a pilot sale, in situ vitrification test. *Geophysics* 60:886–898
- Suzuki K, Toda S, Kusunoki K, Fujimitsu Y, Mogi T, Jomori A (2000) Case studies of electrical and electromagnetic methods applied to mapping active faults beneath the thick quaternary. *Eng Geol* 56:29–45
- Telford WM, Geldart LP, Sheriff RE (1990) *Applied Geophysics*, 2nd edn. Cambridge University Press, Cambridge
- TOKER Drilling and Construction Co., (2003) Ankara Rail Transit System Kızılay Söğütözü Line Construction Works, Soil Investigations Factual Report
- Van Schoor M, Duvenhage D (2000) Comparison of crosshole radio imaging and electrical resistivity tomography for mapping out disseminated sulphide mineralisation at a surface test site in Mpumalanga, South Africa. *Explor Geophys* 30:3–4
- Yalçınar CÇ, Altunel E, Bano M, Meghraoui M, Karabacak V, Akyüz HS (2013) Application of GPR to normal faults in the Büyük Menderes Graben, western Turkey. *J Geodyn* 65:218–227
- Young R, Zhenghan D, Sun J (1995) Interactive Processing of GPR Data. *Lead Edge* 14:175–280
- Zhou B, Dahlin T (2003) Properties and effects of measurement errors on 2D resistivity imaging. *Near Surf Geophys* 1:105–117
- Zhou W, Beck BF, Adams AL (2002) Effective electrode array in mapping karst hazards in electrical resistivity tomography. *Environ Geol* 42:922–928